

Study on low-velocity impact behavior and residual performance prediction of CFRP T-joints

Jianwu Zhou¹, Chao Zhang^{1,2,3}

¹School of Aeronautics, Northwestern Polytechnical University, Xi'an, Shaanxi 710072, China
²School of Civil Aviation, Northwestern Polytechnical University, Xi'an, Shaanxi 710072, China
³Joint International Research Laboratory of Impact Dynamics and Its Engineering Application, Xi'an, Shaanxi 710072, China

Abstract

Composite T-joints are highly susceptible to low-velocity impact, which can significantly affect their residual performance due to the primary working condition of bearing out-of-plane tensile loads. Currently, most methods that employ multiple models or analytical steps to sequentially assess the mechanical properties of composites generally exhibit certain limitations, leaving room for improvement. This study has developed a finite element (FE) model to simulate the low-velocity impact and post-impact tensile behaviors of carbon fiber reinforced polymers (CFRP) T-joints using an integrated analysis method. The model is based on stress failure criteria and continuous stiffness degradation theory and incorporates corrections to the damage variables. Both the low-velocity impact and quasi-static tensile portions of the model are implemented using an explicit solver with the VUMAT subroutine for calculations in Abaqus. The element damage states are transferred between the two models via a Python script, mitigating the inefficiencies and uncontrollable errors associated with the traditional method of transferring element information between multiple models or analytical steps. Finally, the numerical results of mechanical response and damage states are compared with experimental findings from various perspectives. The results show that the model exhibits a maximum error of 10.41% in the main key parameters during low-velocity impact and a maximum error of 10.30% in the ultimate load during post-impact tension. The model's delamination damage state and final tensile failure mode closely align with the experimental results.

Keywords: Adhesive joints; Impact behavior; Residual stress

1. Introduction

The integrated design and manufacturing of composite material structures is a crucial trend in advancing the lightweight development of future aircraft. Composite T-joints, being a quintessential form of integrated structure in aircraft, offer notable advantages including the reduction of fastener count, decreased structural weight, and lowered assembly costs [1-3]. Nevertheless, during actual service operations, T-joints inevitably suffer from external low-velocity impact, such as tools accidentally falling during aircraft maintenance, generating impact energies typically ranging from several joules to tens of joules. Considering that T-joints commonly operate under tensile loading conditions [4,5], conducting a study on the response to low-velocity impacts and the ensuing residual tensile performance holds significant engineering value.

Over the past few decades, researchers have made concerted efforts to address the challenge of damage tolerance in composites by integrating experimental and simulation methods. However, due to the intricate and dispersed nature of composite damage, simulating their dynamic mechanical behavior and predicting overall structural performance remains an arduous task, when it comes to forecasting the residual performance of composites after impact—an issue of paramount importance

that has garnered substantial attention [6]. Currently, the numerical analysis methods commonly employed to predict the performance of composites after low-velocity impact can be categorized into two primary types: the equivalent damage method and restart analysis method. The former method operates on a relatively straightforward principle. It predominantly relies on non-destructive testing results to ascertain the internal damage state of composites post-impact. By simplifying the damage region or equivalently weakening material parameters, it seeks to establish an equivalent substitution between the initial state of the residual performance analysis model and the final state of the low-velocity impact model. However, due to the excessive idealization of equivalent damage, particularly in the presence of highly complex composite failure mechanisms, it may underestimate or even neglect the influence of critical damage modes, resulting in significant deviations in prediction results. As a result, the restart analysis method has garnered increased attention from scholars in recent years.

The restart analysis method entails incorporating setting multiple analysis steps within a single model, where low-velocity impact simulation and post-impact simulation are positioned in successive analysis steps. Post-impact simulation is achieved by resetting boundary conditions and conducting software restart calculations. However, owing to the intricate failure behavior of composites, certain elements may experience substantial mesh distortion during impact without meeting the deletion threshold in the impact model. This poses significant hurdles for mesh convergence in subsequent quasi-static simulations, often necessitating manual searches and deletions prior to implementing subsequent simulations. These laborious manual operations further impede the computational efficiency of the model. In summary, the primary issue with the aforementioned two methods lies in the ineffective transfer of element information, especially element damage states, between adjacent models or analytical steps. Therefore, it is imperative to develop an efficient FE integrated analysis method capable of facilitating seamless and minimal loss transfer of element information, particularly element damage states, between multiple models.

Building upon prior experimental research [7], this study predominantly relies on numerical methods in tandem with the VUMAT subroutine to simulate the mechanical behavior and damage states in CFRP T-joints subjected to low-velocity impact condition (model 1) and subsequent post-impact quasi-static tension (model 2). Furthermore, a Python script serves as a conduit between these two models, facilitating the extraction of final element damage state information from the preceding model and its direct or indirect incorporation into corresponding elements of the subsequent model. Finally, through comparisons with corresponding experimental results from various angles, this method and model's validity is confirmed. This study introduces an integrated modeling method that paves the way for addressing multi-model continuous analysis challenges.

2. The damage model

In this study, the three-dimensional Hashin criterion is implemented, which incorporates the throughthickness normal stress component in matrix failure. Then the intralaminar damage evolution employs the mainstream energy-based linear continuous degradation model, as shown in figure 1.

Since the failure strain of the element is influenced by itself, it is not appropriate to treat the failure strain of the material as a fixed material parameter. Based on Hillerborg's theory of material fracture energy, the characteristic length of the element is incorporated into the stiffness degradation criterion of the material to mitigate the influence of the element size on the failure behavior of the material, and the fracture toughness is considered as a fixed material parameter and uses it to solve for failure strains under different modes.

On the other hand, the built-in cohesive element in Abaqus based on a bilinear traction-separation relationship is adopted to simulate delamination at the interface. The quadratic stress criterion is chosen as the initial criterion for delamination damage. Then the damage evolution of interlaminar materials adopts the Benzeggagh-Kenane failure criterion.

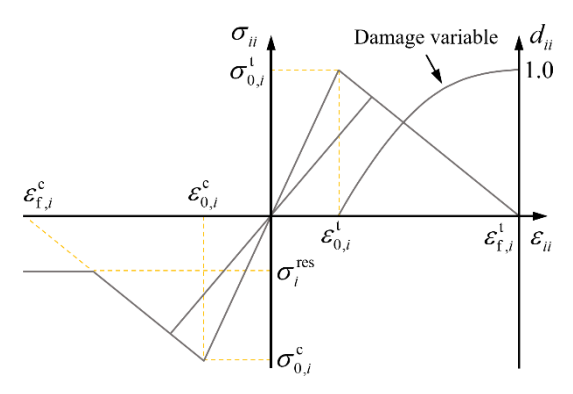


Figure 1 – Schematic diagram of energy-based linear continuous degradation model.

3. Integrated modeling method

As shown in figure 2, this is the complete technical flowchart for FE simulation of low-velocity impact and post-impact tensile testing of a composite T-joint. It can be roughly divided into four modules: pre-processing module, impact module, tensile module, and data connection module.

In the pre-processing module, the T-joint and impactor are created, and they are assigned appropriate material properties, contact properties, and boundary conditions to ensure the model faithfully represents the experimental setup. Both the impact and tensile modules are similar in that they employ Abaqus' explicit solver, in conjunction with a VUMAT subroutine, to carry out calculations. The key distinction is that the latter includes an additional function that writes element information from a specified ".dat" file into the corresponding elements. During the model solving, loads are incrementally applied to obtain material stiffness matrices, strains, stresses, and damage variables for each analysis increment. These results are subsequently compared against with preset conditions to guide the calculation progression.

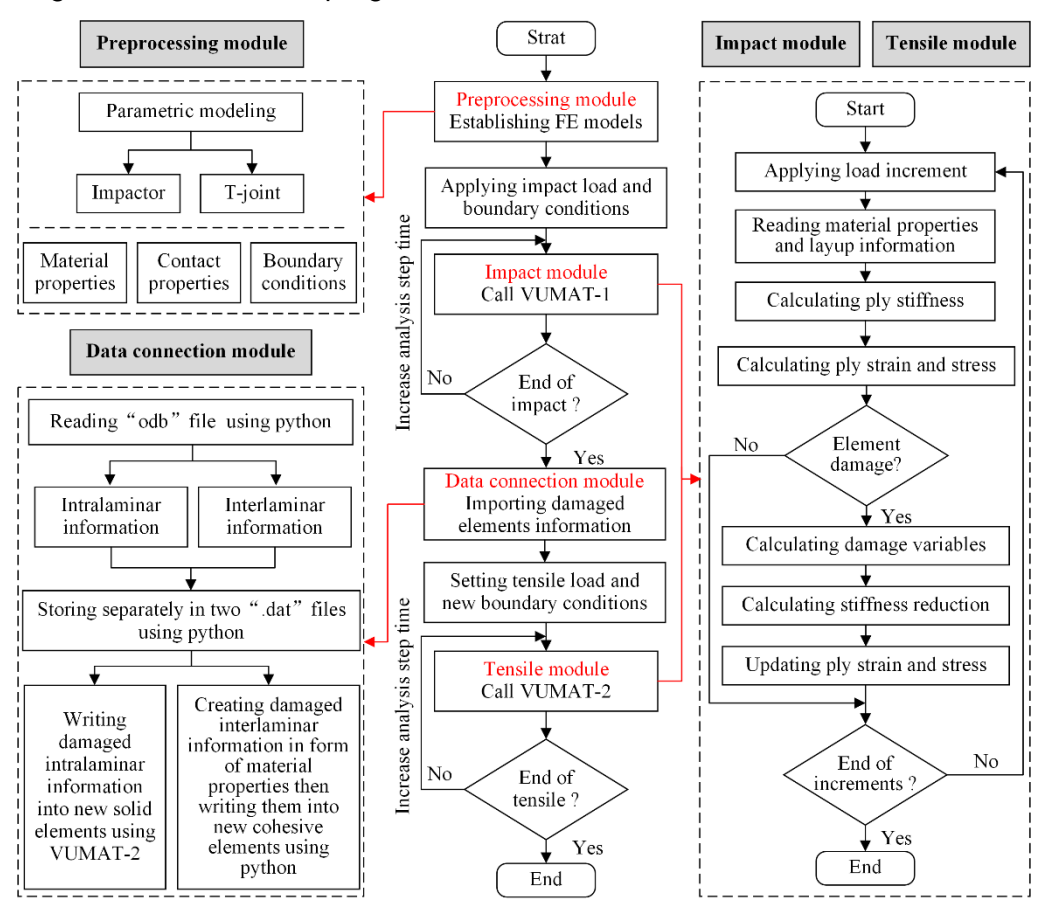


Figure 2 – Overall flowchart of the coordination of various modules.

The data connection module forms the heart of the entire process. It utilizes a Python script to parse the ".odb" file generated from the final impact module calculation results and extracts intralaminar and interlaminar element information into two separate ".dat" files. For intralaminar elements, impact damage is transferred directly following this principle: using the VUMAT subroutine to map the damage state variables obtained from the impact model to the corresponding intralaminar elements in the tensile model. For interlaminar elements, Cohesive elements provided by Abaqus are employed since it's not feasible to directly map the damage state variables using VUMAT. Instead, impact damage is transferred indirectly following this principle: based on the damage state variables of different elements in the impact model, a degraded material model is established for each element. These degraded models are then assigned to the corresponding interlaminar elements in the tensile model in batches. This allows for low loss transmission of all element state information between two adjacent calculation models, as shown in figure 3. Subsequently, by defining new boundary conditions for the tensile test, the calculations can be seamlessly continued.

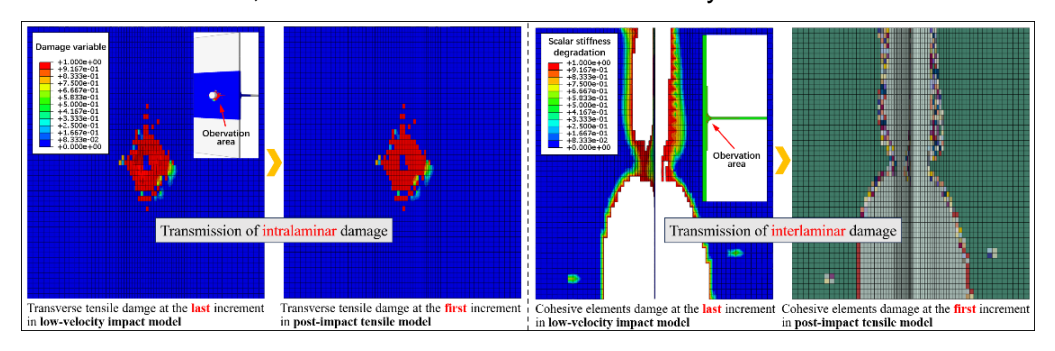


Figure 3 – Low-loss transmission of intralaminar element damage states (taking the matrix tensile as an example) and interlaminar element damage states (taking the bonding interface as an example) between two models.

4. Experiments and FE models

To validate the effectiveness of the integrated model, a comparative study on the low-velocity impact behavior and residual tensile properties of CFRP T-joints was conducted based on our previous experimental work [7]. As shown in figure 4(a), two types of T-joint specimens with a 5 mm fillet radius were manufactured. The key difference between them lies in the utilization of Z-pins for local interlaminar reinforcement.

An IM7/M91 (carbon/epoxy) unidirectional prepreg with a nominal cured ply thickness of 0.175 mm was used to manufacture the skin and L-pieces with corresponding stacking sequences of [45/0/45/90]_{3S} and [45/0/-45/90]_S, respectively. Additionally, the deltoid was filled with the same material oriented along the 90° direction to prevent the formation of a weak resin-rich zone.

The Z-pins were crafted from S35/YH69 (PL/epoxy) prepreg fiber bundles with a diameter of 0.3 mm. They were inserted into the bonding region between the skin and flanges at 4×4 mm intervals. A total of 39 Z-pins were incorporated on each side of the specimen. The specimen with or without Z-pins is referred to as the "Z-pinned T-joint" and "Unpinned T-joint" in this study, respectively.

As depicted in figure 4(b), the T-joint specimen was fixed upside down using a specialized fixture. The Instron Dynatup 9340 impact testing machine with a 10 mm hemispherical impactor and a 5.421 kg impacting part was used to strike at the center of the skin. The anti-rebound device was activated to catch the impacting part and prevent a second impact. Subsequently, post-impact interlaminar damage was meticulously documented for each individual specimen with the aid of ultrasonic C-scan equipment. Following the impact evaluations, quasi-static tensile tests were conducted on both intact specimens and those that had incurred damaged during impact. These tests persisted until complete failure was observed, all while maintaining a controlled tensile rate of 0.5 mm/min, facilitated by a CRIMS DDL100 tensile testing machine, as shown in figure 4(c).

As per the experimental findings, it is evident that damage occurrences are infrequent in both the terminal sections of the skin and the upper portion of the L-pieces in the T-joint during both low-

velocity impact and quasi-static tensile tests. Consequently, to enhance computational efficiency, the progressive damage and failure behavior of the core region is considered, while only elastic behaviors are considered for other regions. The 3D FE models, exemplified by the Z-pinned T-joint, is based on the aforementioned experiments, as shown in figure 4(d). In these models, C3D8R elements are used for the skin, L-pieces and Z-pin, while the C3D6 elements are used for the deltoid region. Zerothickness COH3D8 elements are employed to simulate interface delamination in the core zone. It is important to note that, to ensure the smooth progression of the calculations, an element-based cohesive model is implemented between layers, while a surface-based cohesive model is utilized in the Z-pin regions. Additionally, one element is designated for each layer in the thickness direction. To mitigate the occurrence of zero-energy modes during Abaqus/Explicit simulations, the relaxed stiffness hourglass control method was adopted.

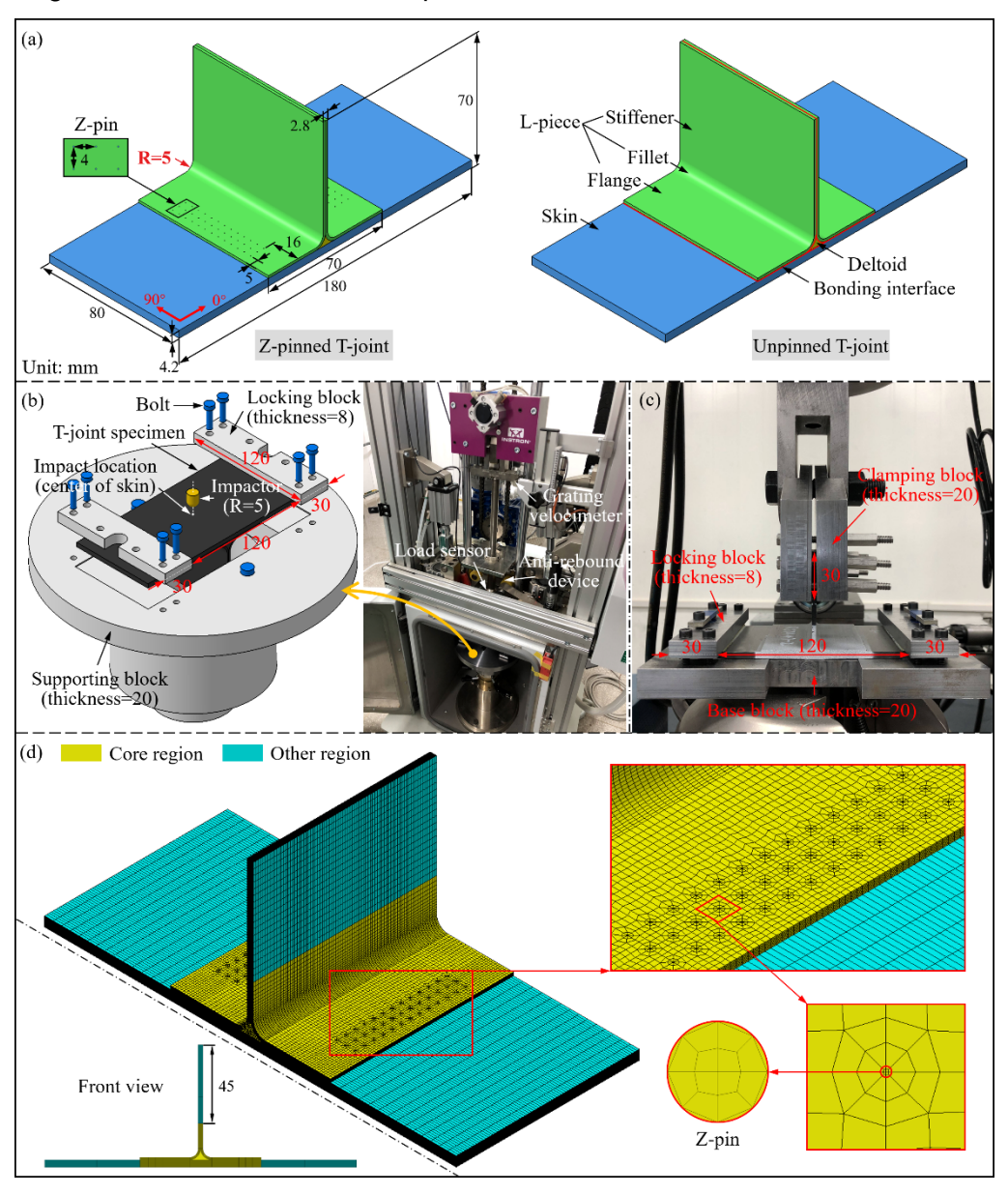


Figure 4 – (a) Two types of T-joint specimens, test Platforms of (b) low-velocity impact and (c) quasi-static tension, (d) 3D FE model of Z-pinned T-joint.

In consideration of computational efficiency, accuracy, and the geometric characteristics of the model, the element size within the core region is primarily set at 0.6×1.0 mm, complemented by 1.0×1.0 mm and 1.0×1.4 mm. Coarser meshing is applied to other regions. The mesh refinement for the deltoid and Z-pin regions is automatically determined based on the aforementioned settings. The

impactor is modeled as an analytical rigid body, with its initial velocity calculated based on the impactor mass and impact energy, which is then applied through a predetermined field. A dynamic penalty function is employed to address the contact problem within the current model, with a friction coefficient set to 0.3.

5. Results and discussion

5.1 Low-velocity impact response prediction of T-joints

When examining the mechanical response to low-velocity impact, a commonly employed research approach involves a quantitative analysis of key parameters, as these parameters offer effective insights into the specimen's impact resistance from various perspectives. Specifically, the Hertzian failure load is often considered the pivotal threshold value for the initiation of extensive delamination damage within the laminate. The maximum load typically exhibits a positive correlation with impact energy, the time duration captures the entire contact process between the impactor and the specimen, the peak energy moment provides a direct reflection of the structural stiffness of the specimen, the final energy accounts for the total energy dissipated by the specimen, the maximum displacement offers insights into the elastic characteristics of the structure, and the final displacement characterizes the extent of damage incurred by the specimen. In addition, fluctuations in load serve as indicators of the intensity of internal damage evolution within the specimen. figure $5(a)\sim(c)$, $(d)\sim(f)$, $(g)\sim(i)$ present typical experimental data alongside corresponding numerical results for impact force-time response curves, transfer energy-time response curves, and impact force-central displacement response curves for T-joints subjected to low-velocity impact at energy levels of 8 J, 15 J, and 25 J, respectively. Both sets of data show high degree of consistency in overall fluctuation patterns and key parameters. The differences between the average experimental results and corresponding numerical results for Hertzian failure load, maximum load, time duration, peak energy moment, final energy, maximum displacement and final displacement are as follow: 47.28%, 4.19%, 3.70%, 0.50%, 5.18%, 1.69%, and 10.41%. Notably, the majority of these differences fall within a reasonable range, with the exception of a pronounced difference in Hertzian failure load, which can be attributed to its relatively small value.

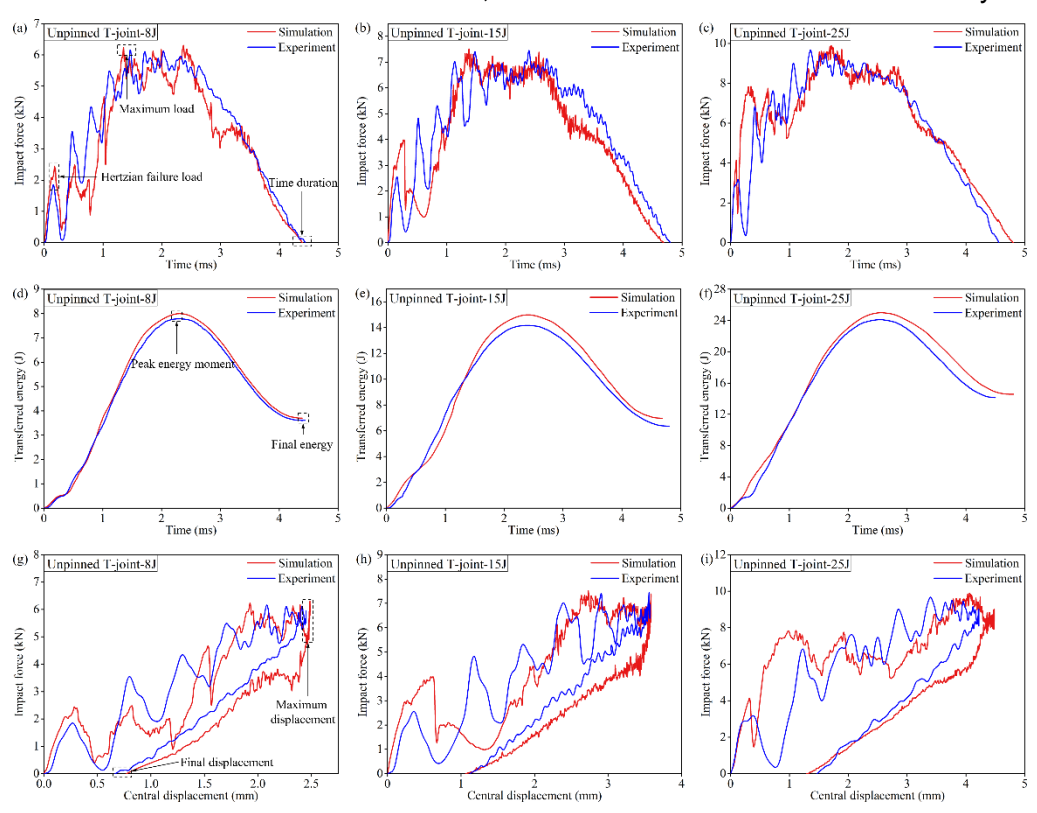


Figure 5 – Typical experimental and numerical results for (a)~(c) impact force-time response curves, (d)~(f) transfer energy-time response curves, and (g)~(i) impact force-central displacement response curves for T-joints during low-velocity impact at 8 J, 15 J, and 25 J energy levels, respectively.

Conversely, the bonding interface stands out as the weakest segment within the entirety of the T-joint, experiencing the most severe delamination damage following low-velocity impact. In prior investigations, non-destructive testing was performed on this region using ultrasonic C-scan equipment. Therefore, the damage outcomes pertaining to the bonding interface within the FE model are extracted and juxtaposed against the experimental findings, as shown in figure 6. The comparative analysis reveals a high degree of similarity between the damage states observed in both the model and the experiments. Notably, after 8 J impact, both exhibit minimal damage. However, following impacts of 15 J or 25 J, both show conspicuous delamination damage, characterized by a distinctive "bow tie" pattern. Higher impact energy caused more serious delamination damage. Nonetheless, some disparities between the model and experimental results exist, primarily concerning the extent of the damaged region. In the experiments, after a 25 J impact, the damage has already spread to a portion of the Z-pin reinforcement region, whereas this is not replicated in the numerical results. This divergence is likely attributed to initial defects arising during specimen preparation, which represents the most significant distinction between the experiment and simulation at present.

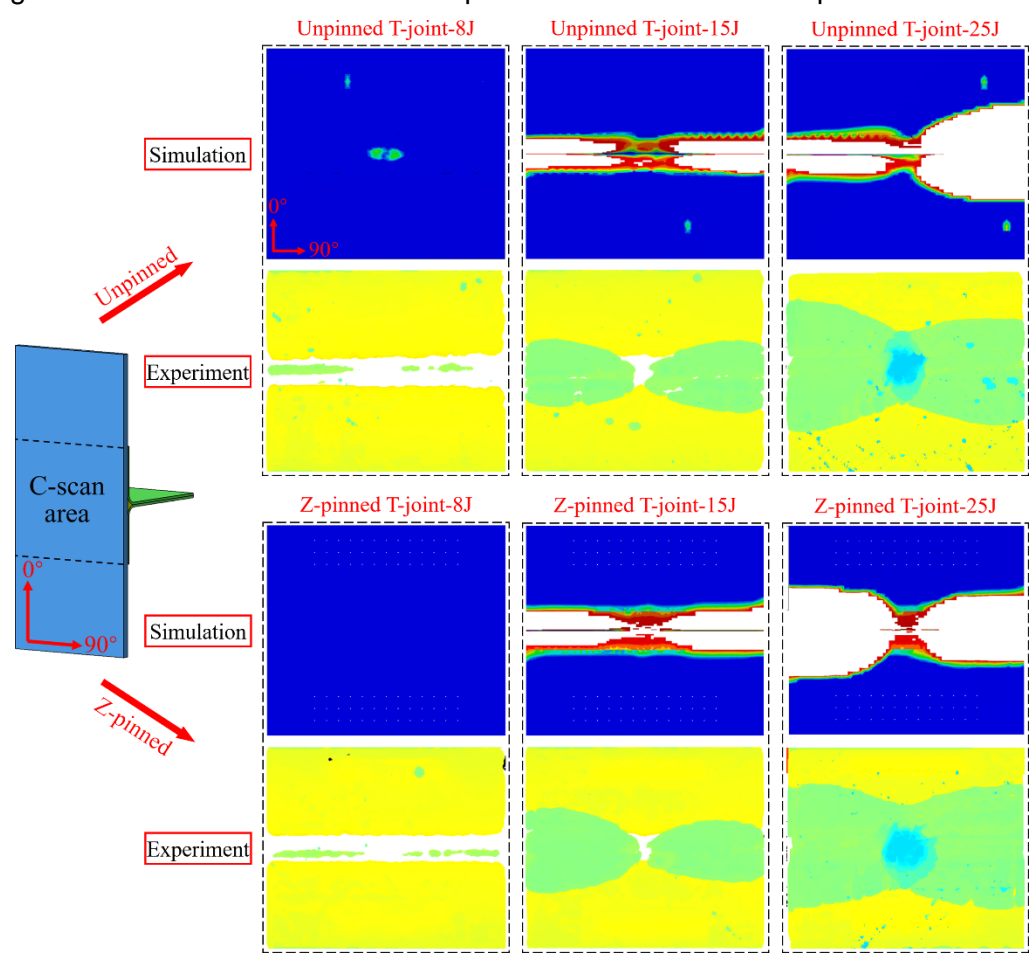


Figure 6 – Comparison of experimental and simulation results of delamination damage region of T-joints after low-velocity impact at different energy levels.

5.2 Residual tensile failure prediction of T-joints

Displayed in figure 7 are the experimental outcomes alongside corresponding numerical results, depicting typical residual tensile load-displacement response curves for T-joints subjected to varying energy impacts. The experimental data reveal that the tensile stiffness of the intact specimen remains virtually unchanged until nearing the ultimate load (figure 7(a)(e)). After an 8 J impact, the specimen only experiences minor tensile stiffness degradation as the load approaches the ultimate value (figure 7(b)(f)). However, specimens subjected to 15 J and 25 J impacts exhibit pronounced stiffness degradation during the later stages of loading (figure 7(c)(d)(g)(h)). These phenomena can primarily be attributed to disparities in the extent of internal damage incurred by the specimens following low-

velocity impact. Notably, all Z-pinned T-joints subjected to 15 J and 25 J impacts exhibit two discernible load recovery stages following the attainment of maximum tensile load. Subsequently, the load stabilizes for a period after reaching near the regional ultimate load (figure 7(g)(h)).

The simulation results align closely with the experimental observations mentioned earlier. Specifically, the differences between the average experimental results and their corresponding numerical counterparts regarding the residual ultimate tensile load of both unpinned T-joint (un) and Z-pinned T-joint (Z) following 0 J, 8 J, 15 J, and 25 J impacts are as follows: 8.92% (un), 6.73% (un), 9.77% (un), 8.08% (un), 3.14% (Z), 6.04% (Z), 9.98% (Z), and 10.30% (Z), respectively. It is worth noting that the simulation results also exhibit a notable load recovery phenomenon. Although the extent of load fluctuation during this stage is considerably greater than what is observed in the experimental data, and the starting positions of multiple load recovery stages are not well distinguished, the phenomenon within the numerical results strongly supports the effectiveness of Z-pin reinforcement in T-joints that have undergone substantial damage.

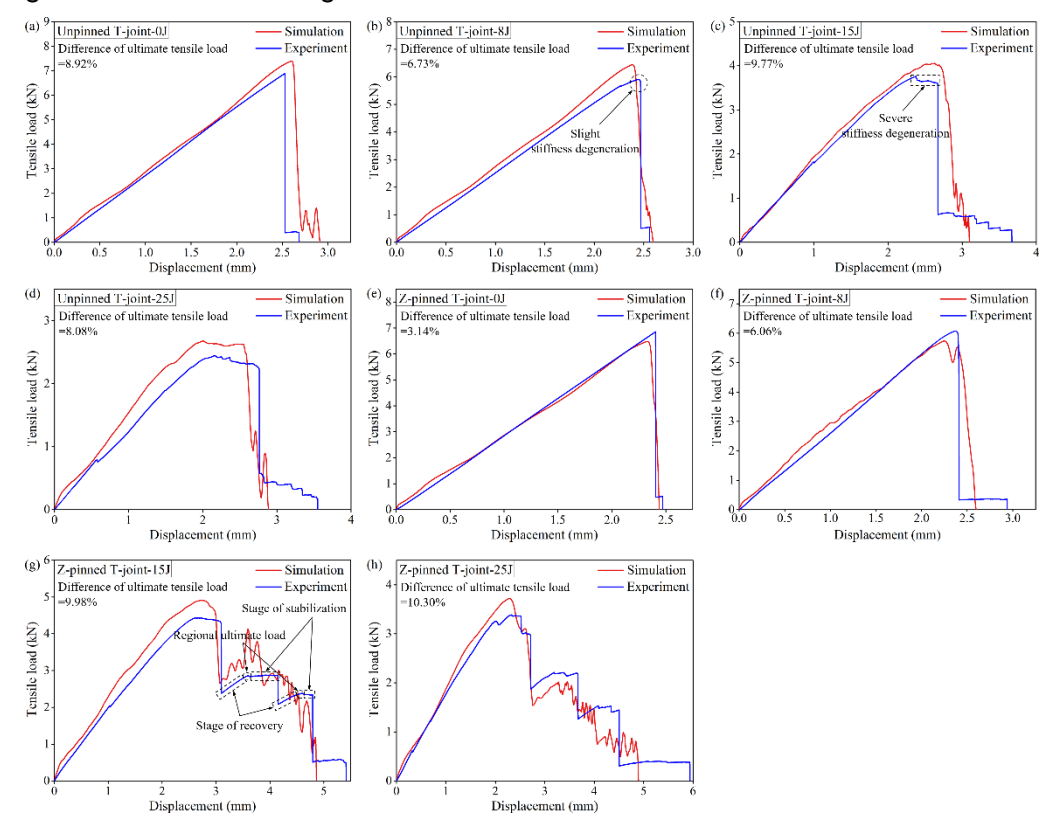


Figure 7 – Typical experimental and numerical results of tensile load-displacement response curves of (a)~(d) unpinned T-joints and (e)~(h) Z-pinned T-joints after different energy impact.

On the other hand, all test specimens, encompassing both intact specimens and those that have sustained damage, manifest two distinct types of failure occurrences. The first type entails the observation of damage extension solely within specific bonding interfaces, more precisely, between the deltoid and one of the fillet regions, and between the skin and both the flange region and the deltoid, as shown in figure 8(a). The second type of failure involves the extension of damage within the fillet regions in addition to the same regions as the first type, as shown in figure 8(c). The FE simulation also replicates these two distinct failure phenomena, as illustrated in figure 8(b)(d).

Upon comparison, it becomes evident that the failure mode of the T-joint obtained through simulation closely aligns with the failure mode observed experimentally, exhibiting only minor discrepancies. Both types of failure phenomena primarily occur during the pull-off process of intact specimens and specimens subjected to an 8 J impact. Meanwhile, the second type of failure phenomenon primarily emerges during the pull-off process of specimens subjected to 15 J or 25 J impacts. An examination of the cross-sectional damage state within the FE model reveals that specimens subjected to 15 J and 25 J impacts exhibit more pronounced delamination damage across multiple layers, including within

the fillet regions (figure 8(f)(g)), whereas specimens subjected to an 8 J impact display only limited damage in these regions (figure 8(e)). Consequently, during the post-impact tensile process, these delaminated regions, in addition to the inherently fragile bonding interface, undergo further extension of delamination damage.

Lastly, the FE model faithfully reproduces the pull-off failure phenomenon of Z-pins in Z-pinned T-joints, as shown in figure 8(h). The outcomes reveal that nearly all Z-pins experience failure through pull-out mechanisms throughout the entire process. Only a minority of Z-pins incur fiber and matrix damage at the end where being pulled out, and the locations of the pull-out events consistently occur within the flange regions. This phenomenon arises from the fact that the skin's thickness is four times that of the L-pieces, endowing the skin with greater capacity to exert constraint force during the load-bearing process of the Z-pin.

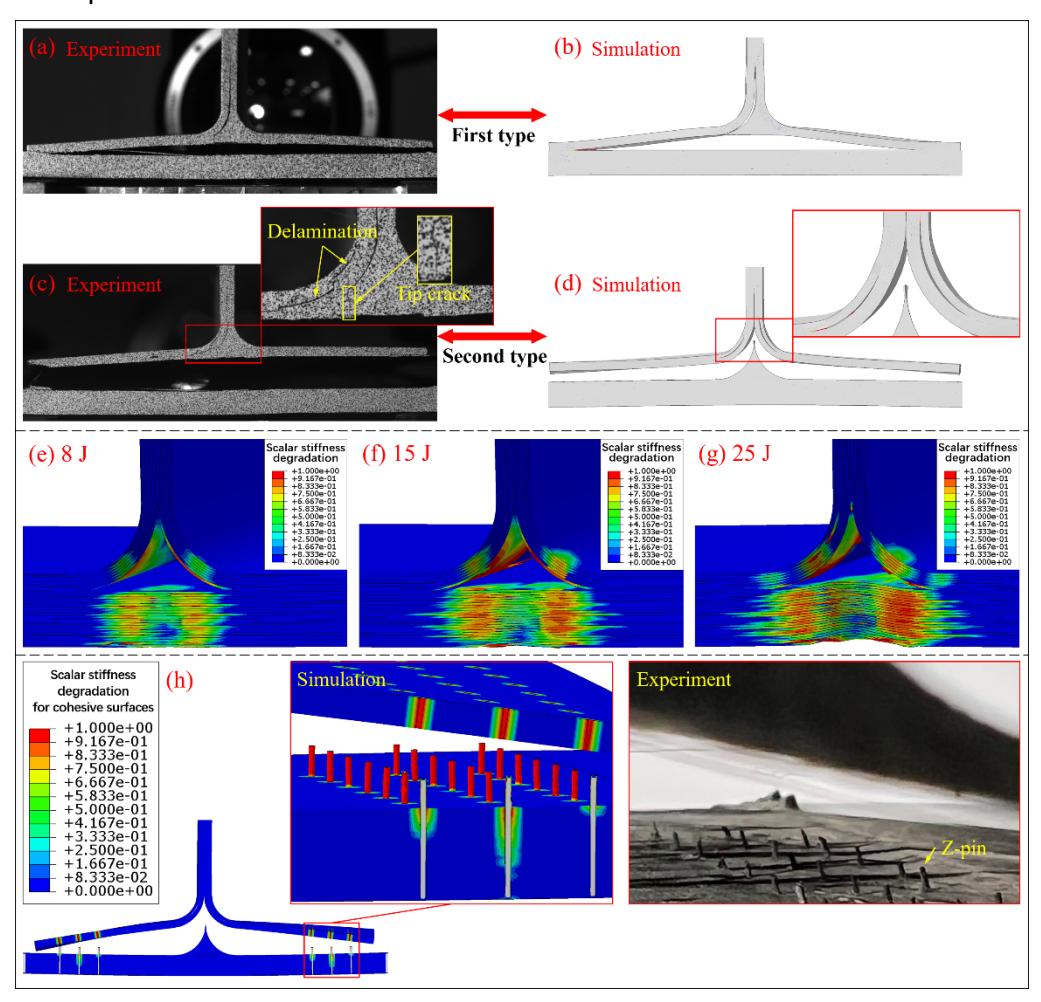


Figure 8 – (a) \sim (d) Comparison of different failure modes during tensile process, (e) \sim (g) difference in distribution of delamination damage regions of T-joints after low-velocity impact, (h) comparison of final failure modes of Z-pin.

6. Conclusions

This study investigates the mechanical response of CFRP T-joints through a new integrated modeling method. Through the study, the following conclusions can be drawn:

(1) By utilizing Python scripts to extract the final element information from the previous model and importing it into the corresponding element of the subsequent model, the damage state of the model can be transferred with low loss. On this basis, the integrated model using VUMAT subroutines for calculation can accurately and efficiently simulate the low-velocity impact behavior of CFRP T-joint and its residual tensile performance after impact. This analytical approach can be extended to nearly all FE simulation problems that involve integrated analysis between two or more models.

- (2) Although Z-pin reinforcement in non-impact region has little effect on the low-velocity impact response of CFRP T-joint and minimal effect on the tensile performance of intact or slightly damaged CFRP T-joint, it can effectively suppress damage extension in the bonding region when low-velocity impact causes significant interlaminar damage. Specifically, after the CFRP T-joint reaches the ultimate load and experiences a sudden drop in load, Z-pin can prevent complete failure and enable it to regain its load-bearing capacity within a certain range.
- (3) The location of interlaminar damage caused by low-velocity impact on CFRP T-joint is a crucial factor in determining the number of damage extension regions during subsequent quasi-static pull-off process. Process defects during manufacturing are also key in determining the exact failure location of the deltoid of CFRP T-joint. These factors jointly dictate the final failure mode of CFRT T-joint. Additionally, the final failure mode for almost all Z-pins is complete pull-out in the flange region of L-pieces, indicating that increasing the thickness of this region can enhance overall interlaminar reinforcement.

Contact Author Email Address

E-mail: Zhoujw@nwpu.edu.cn

Copyright Statement

The authors confirm that they, and/or their company or organization, hold copyright on all of the original material included in this paper. The authors also confirm that they have obtained permission, from the copyright holder of any third party material included in this paper, to publish it as part of their paper. The authors confirm that they give permission, or have obtained permission from the copyright holder of this paper, for the publication and distribution of this paper as part of the ICAS proceedings or as individual off-prints from the proceedings.

References

- [1] Liu H, Liu J, Ding Y, Hall ZE, Kong X, Zhou J, et al. A three-dimensional elastic-plastic damage model for predicting the impact behaviour of fibre-reinforced polymer-matrix composites. *Compos. Part B-Eng.*, No. 201, pp 108389, 2020.
- [2] Yan S, Zeng X, Long A. Meso-scale modelling of 3D woven composite T-joints with weave variations. *Compos. Sci. Technol.*, No. 171 pp 171-179, 2019.
- [3] Zhang H, He R, Hou B, Li Y, Cui H, Yang W. Artificial hail ice impact damage of laminated composite T-joint with stitching reinforcement. *Compos. Struct.*, No. 278, pp 114714, 2021.
- [4] Yan S, Zeng X, Long A. Experimental assessment of the mechanical behaviour of 3D woven composite T-joints. *Compos. Part B-Eng.*, No. 154, pp 108-113, 2018.
- [5] Zhou J, Zhao Z, Shi Y, Wang X, Chen X, Shan C. Hail impact responses and residual tensile properties of CFRP T-joints. *Chinese J. Aeronaut.*, S1000936123000614, 2023.
- [6] Shah SZH, Karuppanan S, Megat-Yusoff PSM, Sajid Z. Impact resistance and damage tolerance of fiber reinforced composites: A review. *Compos. Struct.*, No. 217, pp 100-121, 2019.
- [7] Zhou J, Shi Y, Zuo Y, Shan C, Gu Z. Experimental investigation into influences of Z-pin and deltoid on structural properties and damage tolerance of CFRP T-joints. Compos. Part B-Eng., No. 237, pp 109875, 2022.